

Initial perturbation matters: implications of geometry-dependent universal Kardar-Parisi-Zhang statistics for spatiotemporal chaos

Yohsuke T. Fukai^{1,2,*} and Kazumasa A. Takeuchi^{2,†}

¹*Nonequilibrium Physics of Living Matter RIKEN Hakubi Research Team,
RIKEN Center for Biosystems Dynamics Research,
2-2-3 Minatojima-minamimachi, Chuo-ku, Kobe, Hyogo 650-0047, Japan*

²*Department of Physics, The University of Tokyo, 7-3-1 Hongo, Bunkyo-ku, Tokyo 113-0033, Japan*
(Dated: February 27, 2022)

Infinitesimal perturbations in various systems showing spatiotemporal chaos (STC) evolve following the power laws of the Kardar-Parisi-Zhang (KPZ) universality class. While universal properties beyond the power-law exponents, such as distributions and correlations, and their geometry dependence, are established for random growth and related KPZ systems, the validity of these findings to *deterministic* chaotic perturbations is unknown. Here we fill this gap between stochastic KPZ systems and deterministic STC perturbations by conducting extensive simulations of a prototypical STC system, namely the logistic coupled map lattice. We show that the perturbation interfaces, defined by the logarithm of the modulus of the perturbation vector components, exhibit the universal, geometry-dependent statistical laws of the KPZ class, despite the deterministic nature of STC. We demonstrate that KPZ statistics for three established geometries arise for different initial profiles of the perturbation, namely point (local), uniform, and “pseudo-stationary” initial perturbations, the last being the statistically stationary state of KPZ interfaces given independently of the Lyapunov vector. This geometry dependence lasts until the KPZ correlation length becomes comparable to the system size. Thereafter, perturbation vectors converge to the unique Lyapunov vector, showing characteristic meandering, coalescence, and annihilation of borders of piece-wise regions that remain different from the Lyapunov vector. Our work implies that the KPZ universality for stochastic systems generally characterizes deterministic STC perturbations, providing new insights for STC, such as the universal dependence on initial perturbation and beyond.

Introduction. To understand general laws governing spatially extended dynamical systems, it is insightful to focus on the thermodynamic limit. Successful approaches include applying the concept of phase transition to understand collective states [1–5] and synchronization [6] in large dynamical systems. Considering the infinite-size limit is also crucial for defining the extensivity of chaos, by the existence of a finite density of Lyapunov exponents per degree of freedom [7–9].

In particular, universality associated with scale invariance has successfully provided a general insight for growing infinitesimal perturbations in spatially extended dynamical systems. When a system is showing spatiotemporal chaos (STC), i.e., chaos characterized by spatial and temporal disorder, perturbations given to trajectories typically grow exponentially and fluctuate. Pioneering studies by Pikovsky, Kurths, and Politi [10, 11] revealed that, for a wide range of systems, this growing perturbation belongs to the Kardar-Parisi-Zhang (KPZ) universality class [12], which is one of the most wide-ranging universality classes for various stochastic processes (see reviews [13–19]), including growing interfaces, directed polymers, stochastic particle transport, nonlinear fluctuating hydrodynamics [18, 20], and most recently, to quantum spin chains [21–24], to name but a few.

To be more specific, let us focus on a system showing STC in one-dimensional space. We denote the dynamical variable by $u(x, t) \in \mathbb{R}$, with position $x \in \mathbb{R}$ and time $t \in \mathbb{R}$, and consider an infinitesimal perturbation $\delta u(x, t)$,

growing from a given initial perturbation $\delta u(x, 0)$ applied to the trajectory. Then, Pikovsky and coworkers [10, 11] studied fluctuations of $h(x, t) := \log |\delta u(x, t)|$, which we call the *perturbation interface*, and found universal power laws for the fluctuation amplitude $\sim t^\beta$ and the correlation length $\sim t^{1/z}$, with characteristic exponents $\beta = 1/3$ and $z = 3/2$ of the one-dimensional KPZ class. This emergence of KPZ fluctuations in STC perturbations has been found in a variety of systems, ranging from coupled map lattices (CML) [10, 11, 25–27], a coupled ordinary differential equation [26, 27], partial differential equations [11] to time-delayed systems [11, 27].

However, this connection to the KPZ class has far-reaching implications, beyond the exponents. The understanding on the one-dimensional KPZ class has been completely renewed during the last decades, thanks to remarkable developments by exact solutions [13–19]. One of the most important outcomes was the determination of the distribution and correlation functions of the interface fluctuations, which turned out to be universal yet dependent on the initial condition [13–16, 19]. More specifically, first, we can write down the interface height $h(x, t)$ for infinite-size systems, asymptotically, in the following form:

$$h(x, t) \simeq v_\infty t + (\Gamma t)^{1/3} \chi(X, t), \quad (1)$$

where $\chi(X, t)$ is a stochastic variable discussed below, $X := x/\xi(t)$ is the coordinate rescaled by the correlation length $\xi(t) := \frac{2}{A}(\Gamma t)^{2/3}$, and v_∞, Γ, A are system-

dependent parameters [19, 28]. Then, it has been shown both theoretically [13, 14, 19] and experimentally [19, 29–34] that $\chi(X, t)$ exhibits universal statistical properties, yet these are dependent on the choice of the initial condition $h(x, 0)$. In particular, three canonical cases are known, sometimes referred to as *universality subclasses*: (i) the flat subclass for the flat initial condition $h(x, 0) = 0$; (ii) the circular subclass for wedge or curved initial conditions, e.g., $h(x, 0) = -\kappa|x|$ or $-cx^2$; (iii) the stationary subclass for statistically stationary initial conditions. Note that such initial conditions typically take the form of $h(x, 0) = \sqrt{AB(x)}$, where $B(x)$ is the standard Brownian motion characterized by $\langle [B(x + \ell) - B(x)]^2 \rangle = \ell$ and $B(0) = 0$. This is true exactly of the KPZ equation [12, 19, 35], the prototypical Langevin equation for the KPZ class, and also valid for other models in coarse-grained scales. Then, for each subclass, the one-point distribution of $\chi(0, t \rightarrow \infty)$ is known to be (i) the Gaussian orthogonal ensemble (GOE) Tracy-Widom distribution [36], (ii) the Gaussian unitary ensemble (GUE) Tracy-Widom distribution [37], and (iii) the Baik-Rains distribution [38] (see [13, 14, 16, 19, 39]). This is expressed by $\chi(0, t) \xrightarrow{d} \chi_1, \chi_2, \chi_0$, respectively, where the right-hand side is a random number drawn from each distribution¹ and \xrightarrow{d} denotes convergence in the distribution. These subclasses have also been distinguished and characterized by correlation functions [13–19], which continue attracting considerable attention (e.g., recent developments on time covariance [31, 40–44] and on correlations for general initial conditions [45, 46]).

With this background, the following questions naturally arise: Does this initial-condition dependence of KPZ fluctuations show up in perturbation dynamics of STC? If yes, how? Moreover, since we expect that the vector direction of $\delta u(x, t)$ eventually converges to the unique Lyapunov vector associated with the largest Lyapunov exponent, as Oselsedec’s theorem [47–49] suggests unless the largest exponent is degenerate, how does the initial-condition dependence of $\delta u(x, t)$ reconcile with this fact? In this Letter, we address these questions numerically by an extensive simulation of the CML of the logistic map, a prototypical model showing STC.

Method. We employed the CML of the logistic map as a prototypical model showing STC [50, 51]. The dynamical variables $u(x, t) \in [0, 1]$ are defined for integer x and t , with the periodic boundary condition $u(x, t) = u(\text{mod}(x, L), t)$. Time evolution is set to be

$$u(x, t + 1) = (1 - \epsilon)f(u(x, t)) + \frac{\epsilon}{2}[f(u(x - 1, t)) + f(u(x + 1, t))] \quad (2)$$

$$=: F_x(u(0, t), u(1, t), \dots, u(L - 1, t)), \quad (3)$$

¹ Note $\chi_1 := 2^{-2/3} \chi_{\text{GOE-TW}}$, where $\chi_{\text{GOE-TW}}$ is the standard GOE Tracy-Widom random variable [36].

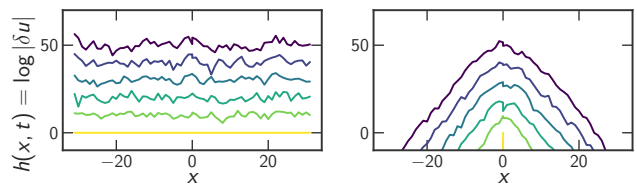


FIG. 1. Typical snapshots of $h(x, t) = \log |\delta u(x, t)|$ from the uniform (left) and point (right) initial perturbations, at $t = 0, 20, \dots, 100$ from bottom to top.

with $f(u) = au(1 - u)$ and parameters ϵ and a . In this Letter, we chose $a = 4$ and $\epsilon = 0.05$, for which this CML shows fully disordered STC [50, 51]. With this trajectory, the evolution of infinitesimal perturbations $\delta u(x, t)$ is given by

$$\delta u(x, t + 1) = \sum_{x'=0}^{L-1} \frac{\partial F_x(u_0, \dots, u_{L-1})}{\partial u_{x'}} \bigg|_{u_i = u(i, t)} \delta u(x', t). \quad (4)$$

To discard the transient before we applied a perturbation at $t = 0$, each simulation started at $t = -T_{\text{warmup}}$ from an initial condition $u(x, -T_{\text{warmup}})$ generated randomly and independently from the uniform distribution in $[0, 1]$. In this Letter, we chose $T_{\text{warmup}} = 1000$ and checked that the histograms of $u(x, t)$ at $t = 0$ and $t = 10^5$ are statistically indistinguishable (Fig. S1 [52]). This suggests that the system is already in the attractor at $t = 0$. We then applied a perturbation $\delta u(x, 0)$ that takes different forms as we describe below. From $\delta u(x, 0)$, we obtained $\delta u(x, t)$ by Eq. (4) and analyzed fluctuations of $h(x, t) = \log |\delta u(x, t)|$.

Uniform and point initial perturbations. We first studied whether perturbation dynamics of STC indeed depends on the initial shape of perturbation, comparing with characteristic statistical properties of the corresponding KPZ subclass. For this, we compare the following two initial conditions, namely the uniform and point initial perturbations, defined by

$$\delta u(x, 0) = \begin{cases} 1, & (\text{uniform}) \\ \delta_{x,0} & (\text{point}). \end{cases} \quad (5)$$

Figure 1 shows typical snapshots of the perturbation interface $h(x, t) = \log |\delta u(x, t)|$ for those initial perturbations. We simulated 2400 and 160000 independent trajectories with $L = 2^{15}$ and $L = 2^{12}$ for the uniform and point perturbations, respectively.

First, we measured the mean height $\langle h(0, t) \rangle$, where $\langle \dots \rangle$ indicates the ensemble average. In the case of the uniform perturbations, we also took the spatial average because of the translational symmetry. As expected, $\langle h(0, t) \rangle$ grows linearly with time, reflecting the exponential growth of the perturbation (Fig. S2 [52]). We also measured the variance $\langle h(0, t)^2 \rangle_c = \langle \delta h(0, t)^2 \rangle$ with $\delta h(x, t) := h(x, t) - \langle h(x, t) \rangle$ and the third- and

fourth-order cumulants, $\langle h(0, t)^3 \rangle_c = \langle \delta h(0, t)^3 \rangle$ and $\langle h(0, t)^4 \rangle_c = \langle \delta h(0, t)^4 \rangle - 3\langle \delta h(0, t)^2 \rangle^2$. The k th-order cumulants ($k = 2, 3, 4$) show power laws $\langle h(0, t)^k \rangle_c \sim t^{k/3}$ characteristic of the KPZ class [Figs. 2(a) and S2 [52]], indicating that this exponent does not depend on the choice of initial perturbation, as expected.

We then investigated the one-point distribution of $h(0, t)$. A convenient way to do so is to measure the skewness $\text{Sk}[h(0, t)] := \langle h(0, t)^3 \rangle_c / \langle h(0, t)^2 \rangle_c^{3/2}$ and the kurtosis $\text{Ku}[h(0, t)] := \langle h(0, t)^4 \rangle_c / \langle h(0, t)^2 \rangle_c^2$. The results in Fig. 2(b) show that those for the uniform initial perturbation converge to the values of the exact solution for the flat KPZ subclass, $\text{Sk}[h(0, t)] \rightarrow \text{Sk}[\chi_1]$ and $\text{Ku}[h(0, t)] \rightarrow \text{Ku}[\chi_1]$, while those for the circular subclass appear for the point initial perturbation, $\text{Sk}[h(0, t)] \rightarrow \text{Sk}[\chi_2]$ and $\text{Ku}[h(0, t)] \rightarrow \text{Ku}[\chi_2]$. These results indicate that the perturbation interfaces from the uniform and point initial perturbations belong to the flat and circular KPZ subclasses, respectively.

To characterize statistical properties further, we estimated the nonuniversal parameters, v_∞ , Γ , and A , following the standard procedures [19, 53]. These parameters are expected to be independent of the choice of initial perturbation [19, 31, 53]. First we estimated the asymptotic growth speed v_∞ , which corresponds to the Lyapunov exponent in the limit $L \rightarrow \infty$. To do so, we used the local Lyapunov exponent $\lambda(t) := \langle \frac{\partial h(0, t)}{\partial t} \rangle$, which satisfies, for sufficiently large systems, the following relation derived from Eq. (1):

$$\lambda(t) = v_\infty + \text{const.} \times t^{-2/3}. \quad (6)$$

Using this, we estimated v_∞ by linear regression of $\lambda(t)$ against $t^{-2/3}$ [Fig. 2(c)]. We thereby obtained $v_\infty = 0.53249(2)$ for the uniform initial perturbation and $v_\infty = 0.53250(7)$ for the point case, where the numbers in the parentheses indicate the estimation uncertainty. This shows, indeed, that v_∞ does not depend on the initial perturbation. Next, we estimated the parameter Γ by $\langle h(0, t)^2 \rangle_c / \langle \chi_j^2 \rangle_c t^{2/3} \simeq \Gamma^{2/3}$ derived from Eq. (1), with $j = 1$ ($j = 2$) for the uniform (point) initial perturbation. Similarly to other examples of KPZ interfaces [19, 31, 54], the quantity in the left-hand side turned out to show finite-time corrections in the order of $\mathcal{O}(t^{-2/3})$ (Fig. S3 [52]). We therefore linearly fitted it against $t^{-2/3}$ and read its intercept, obtaining $\Gamma = 0.1373(5)$ and $0.1369(6)$ for the uniform and point initial perturbations, respectively. From this, we derived the final estimate $\Gamma = 0.1371(9)$. Finally, we estimated A from the infinite-time growth speed for the finite-size systems, or the Lyapunov exponent, $\lambda_\infty(L) := \lim_{t \rightarrow \infty} \langle \frac{\partial h}{\partial t} \rangle$. First, note that Eq. (6) for $\lambda(t)$ is expected to be valid until the correlation length $\xi(t)$ reaches the system size L . Beyond this time, $\lambda(t)$ is expected to deviate from Eq. (6) and converge to $\lambda_\infty(L) \simeq v_\infty - \frac{A\tilde{\lambda}}{L}$, where $\tilde{\lambda}$ is a parameter satisfying $\Gamma = \frac{A^2|\tilde{\lambda}|}{2}$ [19, 53]. Simulating

perturbation interfaces from the uniform initial perturbation (see Table SI [52] for used parameter values), we confirmed that $\lambda_\infty(L)$ indeed depends linearly on L^{-1} [Fig. 2(c) inset]. Therefore, by linear regression, we obtained $A\tilde{\lambda} = 0.0744(3)$ and $v_\infty = 0.5324985(7)$, the latter refining our previous estimates. We then used the estimated values of Γ and $A\tilde{\lambda}$ to obtain A by $A = \frac{2\Gamma}{A\tilde{\lambda}}$.

With those parameters, we defined the rescaled height

$$q(0, t) := \frac{h(0, t) - v_\infty t}{(\Gamma t)^{1/3}} \simeq \chi(0, t) \quad (7)$$

and investigated its statistical properties. Figure 2(d) shows its one-point probability density function (again taking all X for the uniform perturbation). The distributions for the uniform and point initial perturbation agree with those of the exact solutions for the flat and circular subclasses, namely the GOE and GUE Tracy-Widom distributions. Accordingly, the first- to fourth-order cumulants of $q(0, t)$ converge to those of χ_1 and χ_2 , respectively (Fig. S4 [52]). We also measured spatial and temporal correlation functions and found agreement with the known results for the flat and circular subclasses (see Supplemental Text [52]). These results clearly indicate that the statistical properties of perturbation dynamics for the uniform and point initial perturbation are governed by the flat and circular KPZ subclasses, respectively.

Pseudo-stationary initial perturbation. From the viewpoint of dynamical systems theory, the perturbation interfaces are expected to converge to the unique Lyapunov vector (unique at each point in the phase space), associated with the largest Lyapunov exponent [48, 49]. On the other hand, KPZ interfaces generally have a statistically stationary state, characterized by the time-invariance of the equal-time probability distribution of the height fluctuations. For the KPZ equation, such a stationary state is given by the Brownian motion [12, 19, 35], $h(x, \cdot) = \sqrt{AB}(x)$, as already described. This is characterized by the scaling law for the height-difference correlation function

$$C_h(\Delta x, t) := \langle [h(x + \Delta x, t) - h(x, t)]^2 \rangle \simeq A\Delta x, \quad (8)$$

which generally holds in the stationary state of the one-dimensional KPZ class [13–19, 35]. This implies that the stationary state of a model in the one-dimensional KPZ class generally appears as a Brownian motion in coarse-grained scales. However, since the notion of Brownian motion can be defined only by the ensemble of realizations, it does not specify the unique realization corresponding to the Lyapunov vector. In other words, as a deterministic dynamical system, all realizations of the Brownian motion except the one corresponding to the true Lyapunov vector are *not* the stationary state of the perturbation interfaces. It is therefore natural to ask whether such *pseudo-stationary states*, generated randomly irrespective of the state of the dynamical system,

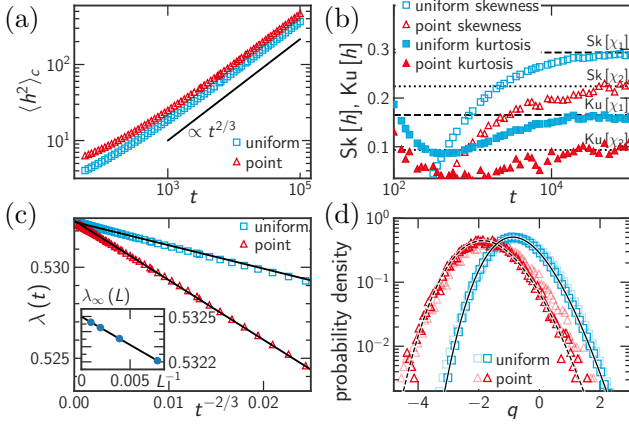


FIG. 2. Results for the uniform and point initial perturbations. (a) The variance of the height $h(0,t)$. The black line is a guide to eyes indicating the power law $t^{2/3}$. (b) The skewness $\text{Sk}[h(0,t)]$ and the kurtosis $\text{Ku}[h(0,t)]$ of the height distribution. The values for χ_1 and χ_2 are shown by the dashed and dotted lines, respectively. (c) The local Lyapunov exponent $\lambda(t)$ plotted against $t^{-2/3}$. The black lines are the results of the linear fit. (inset) The infinite-time Lyapunov exponent $\lambda_\infty(L)$ plotted against L^{-1} . The black line is the result of the linear fit used for the estimation of $A\tilde{\lambda}$ and v_∞ . (d) The rescaled height distribution at $t = 10^3$ (lighter color) and $t = 10^5$ (darker color), for the uniform (turquoise squares) and point (red triangles) perturbations. The probability density function of χ_1 and χ_2 (GOE and GUE Tracy-Widom distributions, respectively) is shown by the solid and dashed lines, respectively.

may exhibit the characteristic fluctuation properties of the stationary KPZ subclass.

To answer this question, we studied the growth of perturbation interfaces starting from pseudo-stationary initial perturbations, given independently of the state of the dynamical system. We prepared a pseudo-stationary initial condition² $h_0(x) = \sqrt{AB}(x)$ with $h_0(0) = 0$, using the estimated value of A , and set the initial perturbation by $\delta u(x, 0) = \exp[h_0(x)]$. Figure 3(a) illustrates the perturbation interface for such a pseudo-stationary initial condition. We simulated 2400 sets of independent trajectories and pseudo-stationary initial perturbations, with $L = 2^{15}$. To evaluate systematic error due to the uncertainty of A in $h_0(x) = \sqrt{AB}(x)$, we also ran simulations with the value of A replaced with its upper and lower bounds of the range of uncertainty, 2400 realizations each.

We first checked the statistical stationarity of perturbation interfaces from such pseudo-stationary initial con-

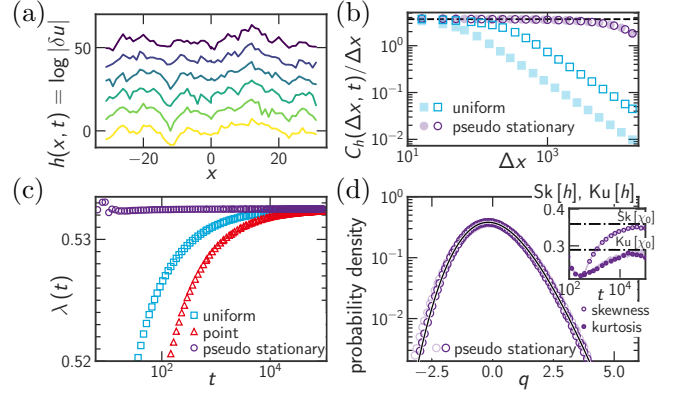


FIG. 3. Results for the pseudo-stationary initial perturbations. (a) Typical snapshots of perturbation interfaces at $t = 0, 20, \dots, 100$ from bottom to top. (b) The height-difference correlation function $C_h(\Delta x, t)/\Delta x$ at $t = 10^4$ (lighter color) and $t = 10^5$ (darker color). The dashed line shows the value of A . (c) The local Lyapunov exponent plotted against time. (d) The height distribution at $t = 10^3$ (lighter color) and $t = 10^5$ (darker color). The solid line shows the Baik-Rains distribution. (inset) The skewness and the kurtosis of $h(x, t)$. The shaded area indicates the systematic error due to the uncertainty of A in $h_0(x) = \sqrt{AB}(x)$ (see text). The dash-dotted lines show the values for the Baik-Rains distribution.

ditions. Figure 3(b) shows that $C_h(\Delta x, t)/\Delta x$ at $t = 10^4$ and 10^5 are identical in the pseudo-stationary case, keeping $C_h(\Delta x, t)/\Delta x \simeq A$ for $\Delta x \ll L$. Figure 3(c) shows that the growth speed, or the local Lyapunov exponent, takes a constant value only after a very short period. These results demonstrate the statistical stationarity of our pseudo-stationary interfaces.

We then compared the statistical properties of the perturbation interfaces with the predictions for the KPZ stationary subclass. In the following, the statistical accuracy was improved by taking advantage of translational symmetry, which guarantees that $h(x, t) - h_0(x)$ is equivalent to $h(0, t)$. We first measured the skewness and kurtosis of $h(0, t)$ and found convergence to those of χ_0 , i.e., the Baik-Rains distribution characterizing the stationary subclass [Fig. 3(d) inset]. We also directly confirmed agreement with the Baik-Rains distribution, by histograms [Fig. 3(e)] and cumulants (Fig. S4 [52]) of the rescaled height $q(0, t)$. Agreement with the stationary KPZ subclass was also confirmed through correlation functions (see Supplemental Text [52]), notably by quantitative agreement to the exact solution of the two-point space-time correlation [55]. These results demonstrate that the perturbation interfaces from the pseudo stationary initial conditions are indeed governed by the stationary KPZ subclass, despite not being stationary for the dynamical system.

Convergence to the Lyapunov vector in finite-size systems. We have shown so far the initial-condition depen-

² Specifically, we generated such a random walk $\tilde{h}_0(x)$ that starts from $\tilde{h}_0(0) = 0$ and steps by $\tilde{h}_0(x+1) = \tilde{h}_0(x) + \sqrt{A}\mathcal{N}$, where \mathcal{N} is a random variable generated from the standard normal distribution. Then, to satisfy the periodic boundary condition, we set $h_0(x) = \tilde{h}_0(x) - \frac{x}{L}[\tilde{h}_0(L) - \tilde{h}_0(0)]$.

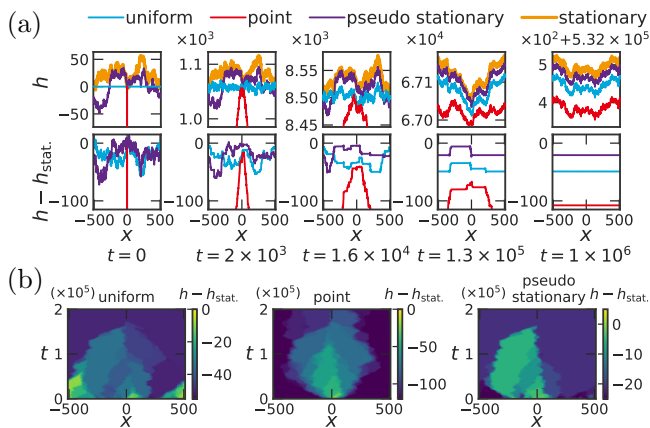


FIG. 4. Convergence of the perturbation interfaces to the Lyapunov vector. (a) Typical snapshots, taken at time indicated below each panel, are shown. (b) Typical evolution of $h(x, t) - h_{\text{stat.}}(x, t)$.

dence of perturbation vectors, focusing on the three cases corresponding to the KPZ subclasses. On the other hand, for finite-size systems, we expect that the direction of the perturbation vectors eventually converges to that of the unique Lyapunov vector [48, 49], whence the initial-condition dependence is lost. This is expected to happen when the correlation length $\xi(t)$ reaches the system size L . Here we investigated how this happens for the three studied initial perturbations, using the same system but with $L = 10^{10}$. With this size, the correlation length $\xi(t)$ reaches L at $t^* := \Gamma^{-1}(\frac{AL}{2})^{3/2} \approx 6 \times 10^5$.

To obtain the Lyapunov vector, we started simulations from $t = -T_{\text{warmup}} - t_0$ with $t_0 := 6 \times 10^6 (\gg t^*)$. After discarding the trajectory's transient for T_{warmup} time steps, we applied a uniform perturbation $\delta u_0(x, -t_0) = 1$ and let it evolve for t_0 time steps. Then we defined $h_{\text{stat.}}(x, t) := \log |\delta u_0(x, t)| - \log |\delta u_0(0, 0)|$, which is the interface corresponding to the Lyapunov vector and we call it the *stationary* perturbation interface. We compared it with the uniform, point, and pseudo-stationary interfaces $h(x, t)$ obtained for the same trajectory, and found that these indeed converge to $h_{\text{stat.}}(x, t)$ up to a constant shift which disappears by normalization of $\delta u(x, t)$ [Fig. 4(a)]. Interestingly, before this convergence, the difference $h(x, t) - h_{\text{stat.}}(x, t)$ consists of piecewise plateaus during this convergence, reminiscent of the difference between the first and subsequent Lyapunov vectors [26]. The plateau edges meander in an apparently random manner, coalesce, and eventually annihilate [Fig. 4(b)].

Summary and discussion. In summary, using the logistic map CML as a prototypical model showing STC, we studied the distribution and correlation properties of perturbation vectors, for the following three types of initial perturbations: uniform, point, and pseudo-stationary. Focusing on the one-point distribution and

two-point correlations, we showed clear evidence of agreement with the flat, circular, and stationary subclasses of the KPZ class, respectively. Since the KPZ exponents have been reported for perturbations in various STC systems [10, 11, 27], it is reasonable to believe the generality of our results. In the pseudo-stationary case, the fact that such a perturbation was not the Lyapunov vector and therefore not stationary for the dynamical system turned out not to affect the statistical properties as the stationary KPZ subclass. These results indicate that the deterministic nature of dynamical systems does not affect the universal statistical properties of the KPZ class, which usually describe stochastic systems. When the correlation length eventually reaches the system size, the perturbation interfaces from different initial perturbations converged to the unique stationary interface up to constant shifts, unlike the statistical interface growth. This convergence is driven by intricate meandering, coalescence, and eventual annihilation of plateau borders seen in the height difference from the stationary interface.

Although we studied only the three types of initial perturbations in this work, the KPZ theory allows us to deal with even general initial perturbations, via what is called the *KPZ variational formula* [34, 56–58]. We expect that we can handle the one-point distribution of perturbation vectors for arbitrary initial conditions, by using the numerical method proposed in [34] and by estimating nonuniversal parameters according to the procedure described in this Letter.

Recent studies have shown that the concept of the KPZ subclasses is also useful for understanding deterministic fluctuations of STC itself, in the Kuramoto-Sivashinsky equation [59], in anharmonic chains [18, 20, 60], in a discrete Gross-Pitaevskii equation [61], etc. We hope that this line of research will continue providing new insights for spatially extended dynamical systems.

Acknowledgments. We thank K. Kawaguchi and S. Ito for useful discussions on the Brownian initial condition with periodic boundary conditions. We are grateful to M. Prähofer and H. Spohn for the theoretical curves of the Baik-Rains and Tracy-Widom distributions and that of the stationary two-point correlation function, which are made available online [62], and to F. Bornemann for the curves of the Airy_1 and Airy_2 covariance, evaluated by his algorithm in [63]. This work is supported in part by KAKENHI from Japan Society for the Promotion of Science (Grant Nos. JP17J05559, JP25103004, JP19H05800, JP20H01826).

* ysk@yukai.net

† kat@kaztake.org

[1] I. S. Aranson and L. Kramer, Rev. Mod. Phys. **74**, 99

- (2002).
- [2] H. Chaté and P. Manneville, Phys. Rev. Lett. **58**, 112 (1987).
 - [3] H. Chaté and P. Manneville, Physica D **32**, 409 (1988).
 - [4] J. Miller and D. A. Huse, Phys. Rev. E **48**, 2528 (1993).
 - [5] P. Marcq, H. Chaté, and P. Manneville, Phys. Rev. Lett. **77**, 4003 (1996); Phys. Rev. E **55**, 2606 (1997).
 - [6] A. Pikovsky, M. Rosenblum, and J. Kurths, *Synchronization: A Universal Concept in Nonlinear Sciences*, Cambridge Nonlinear Science Series (Cambridge Univ. Press, New York, 2003).
 - [7] D. Ruelle, Commun. Math. Phys. **87**, 287 (1982).
 - [8] P. Manneville, in *Macroscopic Modelling of Turbulent Flows*, Lecture Notes in Physics, edited by U. Frisch, J. B. Keller, G. C. Papanicolaou, and O. Pironneau (Springer, Berlin, Heidelberg, 1985) pp. 319–326.
 - [9] D. A. Egolf, I. V. Melnikov, W. Pesch, and R. E. Ecke, Nature **404**, 733 (2000).
 - [10] A. S. Pikovsky and J. Kurths, Phys. Rev. E **49**, 898 (1994).
 - [11] A. Pikovsky and A. Politi, Nonlinearity **11**, 1049 (1998).
 - [12] M. Kardar, G. Parisi, and Y.-C. Zhang, Phys. Rev. Lett. **56**, 889 (1986).
 - [13] T. Kriecherbauer and J. Krug, J. Phys. A: Math. Theor. **43**, 403001 (2010).
 - [14] I. Corwin, Random Matrices Theory Appl. **01**, 1130001 (2012).
 - [15] J. Quastel and H. Spohn, J. Stat. Phys. **160**, 965 (2015).
 - [16] T. Halpin-Healy and K. A. Takeuchi, J. Stat. Phys. **160**, 794 (2015).
 - [17] T. Sasamoto, Prog. Theor. Exp. Phys. **2016**, 022A01 (2016).
 - [18] H. Spohn, in *Stochastic Processes and Random Matrices: Lecture Notes of the Les Houches Summer School*, Vol. 104, edited by G. Schehr, A. Altland, Y. V. Fyodorov, N. O’Connell, and L. F. Cugliandolo (Oxford University Press, Oxford, 2017) pp. 177–227.
 - [19] K. A. Takeuchi, Physica A **504**, 77 (2018).
 - [20] H. Spohn, in *Thermal Transport in Low Dimensions*, Lecture Notes in Physics No. 921, edited by S. Lepri (Springer International Publishing, Cham, 2016) pp. 107–158.
 - [21] M. Ljubotina, M. Žnidarič, and T. Prosen, Phys. Rev. Lett. **122**, 210602 (2019).
 - [22] A. Scheie, N. E. Sherman, M. Dupont, S. E. Nagler, M. B. Stone, G. E. Granroth, J. E. Moore, and D. A. Tennant, Nat. Phys. **17**, 726 (2021).
 - [23] D. Wei, A. Rubio-Abadal, B. Ye, F. Machado, J. Kemp, K. Srakaew, S. Hollerith, J. Rui, S. Gopalakrishnan, N. Y. Yao, I. Bloch, and J. Zeiher, (2021), arXiv:2107.00038.
 - [24] V. B. Bulchandani, S. Gopalakrishnan, and E. Ilievski, (2021), arXiv:2103.01976.
 - [25] I. G. Szendro, D. Pazó, M. A. Rodríguez, and J. M. López, Phys. Rev. E **76**, 025202 (2007).
 - [26] D. Pazó, I. G. Szendro, J. M. López, and M. A. Rodríguez, Phys. Rev. E **78**, 016209 (2008).
 - [27] D. Pazó, J. M. López, and A. Politi, Phys. Rev. E **87**, 062909 (2013).
 - [28] M. Prähofer and H. Spohn, Physica A **279**, 342 (2000).
 - [29] K. A. Takeuchi and M. Sano, Phys. Rev. Lett. **104**, 230601 (2010).
 - [30] K. A. Takeuchi, M. Sano, T. Sasamoto, and H. Spohn, Sci. Rep. **1**, 34 (2011).
 - [31] K. A. Takeuchi and M. Sano, J. Stat. Phys. **147**, 853 (2012).
 - [32] Y. T. Fukai and K. A. Takeuchi, Phys. Rev. Lett. **119**, 030602 (2017).
 - [33] T. Iwatsuka, Y. T. Fukai, and K. A. Takeuchi, Phys. Rev. Lett. **124**, 250602 (2020).
 - [34] Y. T. Fukai and K. A. Takeuchi, Phys. Rev. Lett. **124**, 060601 (2020).
 - [35] A.-L. Barabási and H. Eugene Stanley, *Fractal Concepts in Surface Growth* (Cambridge University Press, New York, NY, USA, 1995).
 - [36] C. A. Tracy and H. Widom, Commun. Math. Phys. **177**, 727 (1996).
 - [37] C. A. Tracy and H. Widom, Commun. Math. Phys. **159**, 151 (1994).
 - [38] J. Baik and E. M. Rains, J. Stat. Phys. **100**, 523 (2000).
 - [39] M. Prähofer and H. Spohn, Phys. Rev. Lett. **84**, 4882 (2000).
 - [40] P. L. Ferrari and H. Spohn, Symmetry Integrability Geom. Methods Appl. **12**, 074 (2016).
 - [41] J. De Nardis, P. Le Doussal, and K. A. Takeuchi, Phys. Rev. Lett. **118**, 125701 (2017).
 - [42] K. Johansson, Probab. Theory Related Fields **175**, 849 (2019).
 - [43] K. Johansson and M. Rahman, Commun. Pure Appl. Math. (2021), 10.1002/cpa.21980.
 - [44] Z. Liu, (2019), arXiv:1907.09876.
 - [45] I. Corwin, J. Quastel, and D. Remenik, J. Stat. Phys. **160**, 815 (2015).
 - [46] D. Dauvergne, J. Ortmann, and B. Virág, (2019), arXiv:1812.00309.
 - [47] V. I. Oseledec, Trans. Moscow Math. Soc. **19**, 197 (1968).
 - [48] J. P. Eckmann and D. Ruelle, Rev. Mod. Phys. **57**, 617 (1985).
 - [49] P. V. Kuptsov and U. Parlitz, J. Nonlinear Sci. **22**, 727 (2012).
 - [50] K. Kaneko, Physica D **34**, 1 (1989).
 - [51] K. Kaneko, *Theory and applications of coupled map lattices* (Wiley, Chichester, New York, 1993).
 - [52] See Supplemental Material for Supplemental Text, Table SI and Figs. S1, S2, S3, S4, S5 and S6, which includes Refs. [64–67].
 - [53] J. Krug, P. Meakin, and T. Halpin-Healy, Phys. Rev. A **45**, 638 (1992).
 - [54] P. L. Ferrari and R. Frings, J. Stat. Phys. **144**, 1123 (2011).
 - [55] M. Prähofer and H. Spohn, J. Stat. Phys. **115**, 255 (2004).
 - [56] J. Quastel and D. Remenik, in *Topics in Percolative and Disordered Systems* (Springer, New York, NY, 2014) pp. 121–171.
 - [57] I. Corwin, Z. Liu, and D. Wang, Ann. Appl. Probab. **26**, 2030 (2016).
 - [58] J. Quastel and D. Remenik, Trans. Amer. Math. Soc. **371**, 6047 (2019).
 - [59] D. Roy and R. Pandit, Phys. Rev. E **101**, 030103 (2020).
 - [60] C. B. Mendl and H. Spohn, Phys. Rev. E **93**, 060101 (2016).
 - [61] M. Kulkarni, D. A. Huse, and H. Spohn, Phys. Rev. A **92**, 043612 (2015).
 - [62] Theoretical curves available in the following URL were used: <https://www-m5.ma.tum.de/KPZ>.
 - [63] F. Bornemann, Math. Comput. **79**, 871 (2010).
 - [64] T. Sasamoto, J. Phys. A: Math. Gen. **38**, L549 (2005).

- [65] A. Borodin, P. L. Ferrari, M. Prähofer, and T. Sasamoto, J. Stat. Phys. **129**, 1055 (2007).
- [66] M. Prähofer and H. Spohn, J. Stat. Phys. **108**, 1071 (2002).
- [67] J. Baik, P. L. Ferrari, and S. Pécché, Commun. Pure Appl. Math. **63**, 1017 (2010).

Supplemental Material for Initial perturbation matters: implications of geometry-dependent universal Kardar-Parisi-Zhang statistics for spatiotemporal chaos

Yohsuke T. Fukai^{1,2,*} and Kazumasa A. Takeuchi^{2,†}

¹*Nonequilibrium Physics of Living Matter RIKEN Hakubi Research Team,
RIKEN Center for Biosystems Dynamics Research,*

2-2-3 Minatogima-minamimachi, Chuo-ku, Kobe, Hyogo 650-0047, Japan

²*Department of Physics, The University of Tokyo, 7-3-1 Hongo, Bunkyo-ku, Tokyo 113-0033, Japan*
FEBRUARY 27, 2022

SUPPLEMENTAL TEXT ON UNIVERSAL CORRELATION FUNCTIONS

Here we describe some notable predictions on correlation functions for the three KPZ subclasses, and the results of our data from the perturbation interfaces. As described in the Letter, in the one-dimensional KPZ class, the height $h(x, t)$ is expected to take the following form for large t :

$$h(x, t) \simeq v_\infty t + (\Gamma t)^{1/3} \chi(X, t), \quad (S1)$$

where $\chi(X, t)$ is the rescaled random variable and $X := x/\xi(t)$ is the coordinate rescaled by the correlation length $\xi(t) := \frac{2}{A}(\Gamma t)^{2/3}$. The one-point distribution of $\chi(0, t)$ (and also for general X if properly rescaled) is known to converge to the GOE Tracy-Widom distribution for the flat subclass, the GUE Tracy-Widom distribution for the circular subclass, and the Baik-Rains distribution for the stationary subclass. This is expressed by $\chi(0, t) \xrightarrow{d} \chi_1, \chi_2, \chi_0$. In fact, equal-time multi-point distributions of $\chi(X, t)$ are also known and expressed as follows:

$$\chi(X, t) \xrightarrow{d} \begin{cases} \mathcal{A}_1(X) & (\text{flat}) \\ \mathcal{A}_2(X) - X^2 & (\text{circular}) \\ \mathcal{A}_0(X) & (\text{stationary}) \end{cases} \quad (S2)$$

in terms of certain stochastic processes called the Airy_1 process $\mathcal{A}_1(X)$ [1, 2], the Airy_2 process $\mathcal{A}_2(X)$ [3], and the $\text{Airy}_{\text{stat}}$ process $\mathcal{A}_0(X)$ [4], though the $\text{Airy}_{\text{stat}}$ process is essentially the double-sided Brownian motion plus a nontrivial random shift [5]. Compared with equal-time properties, two-time correlation of $\chi(X, t)$ has been a challenging problem, but it has also been shown to have distinct properties among the three subclasses [6–8] and some rigorous results are available now [9–11]. Besides, for the stationary KPZ subclass, covariance of the height or the height gradient between points (x, t) and $(0, 0)$ in space-time has been studied and the exact solutions are available [12].

To characterize these multi-point correlations from data, it is convenient to define the rescaled height

$$q(X, t) := \frac{h(X\xi(t), t) - v_\infty t}{(\Gamma t)^{1/3}} \simeq \chi(X, t). \quad (S3)$$

With this, we define the spatial covariance

$$\begin{aligned} C_s(\Delta X, t) &:= \text{Cov}[q(\Delta X, t), q(0, t)] \\ &\simeq \text{Cov}[\chi(\Delta X, t), \chi(0, t)] \end{aligned} \quad (S4)$$

and the temporal covariance

$$\begin{aligned} C_t(t, t_0) &:= \text{Cov}[q(0, t + t_0), q(0, t_0)] \\ &\simeq \text{Cov}[\chi(0, t + t_0), \chi(0, t_0)] \end{aligned} \quad (S5)$$

where $\text{Cov}[B, C] := \langle BC \rangle - \langle B \rangle \langle C \rangle$ is the covariance between B and C . Then, the spatial covariance $C_s(\Delta X, t)$ can be compared with the theoretical curves for the covariance of the Airy_1 and Airy_2 processes, which were made available by Bornemann [13] by numerical evaluation of the theoretical formula. Concerning the temporal covariance,

the theoretical functional form that can be compared with data is available only for the stationary subclass [7] to our knowledge. However, the power laws describing the decay of the temporal covariance are available for all the three subclasses [6–8], as follows:

$$C_t(t, t_0) \sim \begin{cases} (t/t_0)^{-1} & \text{(flat),} \\ (t/t_0)^{-1/3} & \text{(circular),} \\ (t/t_0)^{-1/3} & \text{(stationary).} \end{cases} \quad (\text{S6})$$

For the uniform and point initial perturbations, we measured the spatial covariance $C_s(\Delta X, t)$ and found agreement with the Airy_1 and Airy_2 covariance, respectively [Fig. S5(a)]. We also measured the temporal covariance $C_t(t, t_0)$ and found the power laws $(t/t_0)^{-1}$ and $(t/t_0)^{-1/3}$ for the uniform and point perturbations, respectively (Fig. S6). These constitute further evidence for the conclusion drawn in the Letter, that the perturbation interfaces for the uniform and point initial perturbations are described by the flat and circular KPZ subclasses, respectively.

For the pseudo-stationary initial perturbations, we measured the two-point height-gradient correlation function, defined by

$$C_{ds}(\Delta X, t) := 2 \left\langle \frac{\partial q}{\partial X}(\Delta X, t) \frac{\partial q}{\partial X}(0, t) \right\rangle. \quad (\text{S7})$$

Here, we took both the ensemble average and the spatial average, using the fact that $h(x, t) - h_0(x)$ is statistically equivalent to $h(0, t)$. Then we found agreement with the exact solution $g''(\cdot)$ by Prähofer and Spohn [12] [Fig. S5(b)]. We also measured the temporal covariance $C_t(t, t_0)$ and found the predicted power law $(t/t_0)^{-1/3}$ (Fig. S6). These demonstrate that the perturbation interfaces from the pseudo-stationary initial conditions are indeed described by the stationary KPZ subclass, as concluded in the Letter.

SUPPLEMENTAL FIGURES

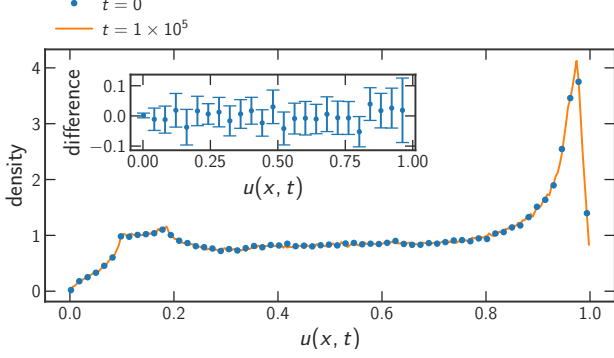


FIG. S1. The histogram of the dynamical variable $u(x, t)$, at $t = 0$ and $t = 1 \times 10^5$ with $T_{\text{warmup}} = 1000$ (see the main text). The inset shows the difference in the probability density, where the error bars indicate the standard error.

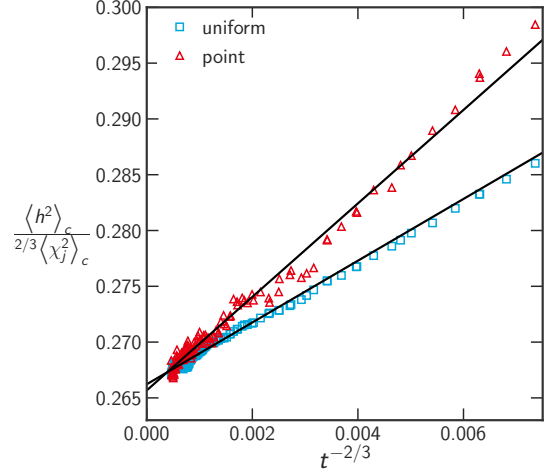


FIG. S3. The variance of the height $\langle h(0, t)^2 \rangle_c$ rescaled by $t^{2/3} \langle \chi_j^2 \rangle_c$, where $j = 1$ ($j = 2$) for the uniform (point) initial perturbation. The black solid lines are linear fits used for the estimation of Γ .

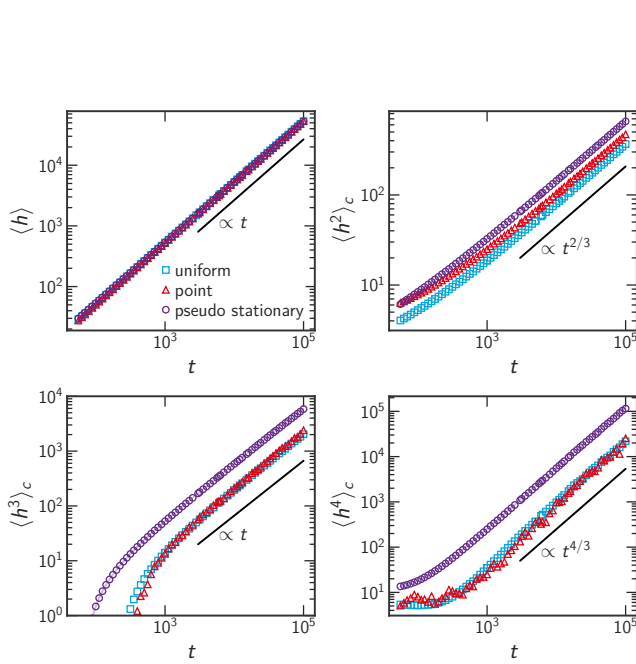


FIG. S2. The cumulants of the height, $\langle h(0, t)^k \rangle_c$, for the uniform, point, and pseudo-stationary initial perturbations ($k = 1, 2, 3, 4$). The black solid lines are guides to the eyes.

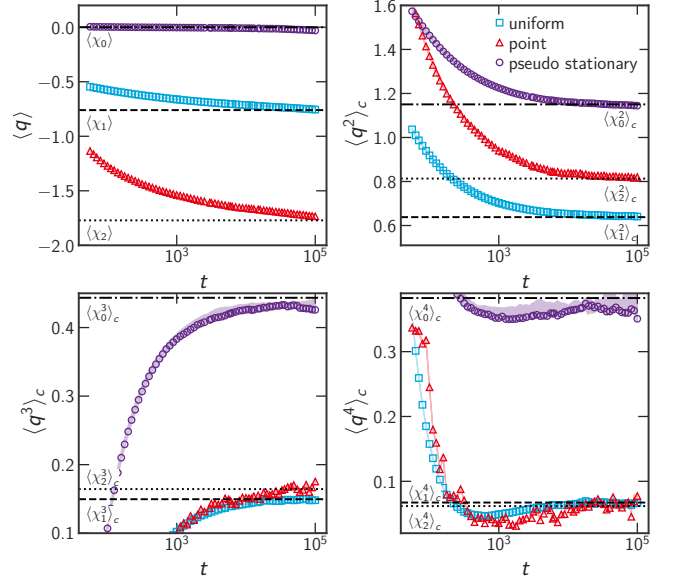


FIG. S4. The cumulants of the rescaled height $\langle q(0, t)^k \rangle_c$ ($k = 1, 2, 3, 4$). The shaded area for the pseudo-stationary data indicates the range of the systematic uncertainty due to the parameter estimation. The values for χ_1 , χ_2 , and χ_0 are shown by the dashed, dotted, and dash-dotted lines, respectively.

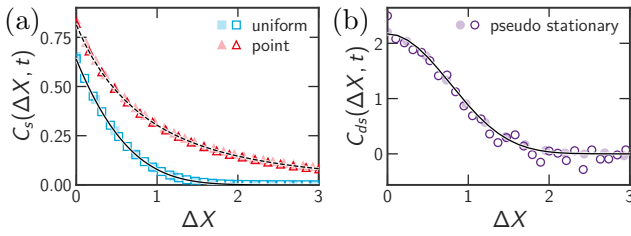


FIG. S5. The spatial covariance for the uniform and point perturbations (a) and the two-point height-gradient covariance for the pseudo-stationary perturbations (b). (a) The spatial covariance $C_s(\Delta X, t)$ at $t = 10^4$ (lighter color) and $t = 10^5$ (darker color), for the uniform (turquoise squares) and point (red triangles) perturbations. The covariance of Airy_1 and Airy_2 processes is shown by the solid and dashed lines, respectively. (b) The two-point height-gradient covariance $C_{ds}(\Delta X, t)$ for the pseudo-stationary perturbations, at $t = 10^4$ (lighter color) and $t = 10^5$ (darker color), compared with the exact solution $g''(\Delta X)$ (solid line).

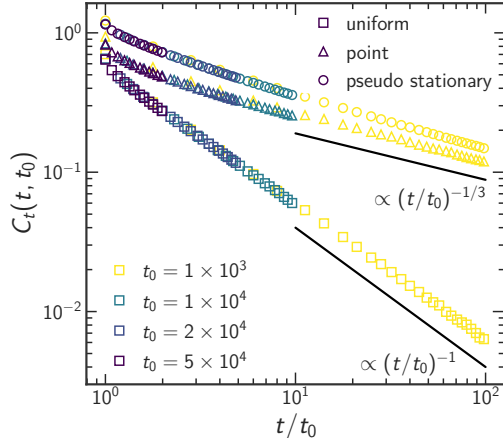


FIG. S6. The temporal covariance $C_t(t, t_0)$. The black lines are guides to the eyes.

SUPPLEMENTAL TABLES

L	T	samples
128	1448154	12000
256	40960000	480
512	11585237	480
1024	32768000	480

TABLE SI. The simulation parameters used to estimate $A\tilde{\lambda}$. Here, T is the number of time steps.

* ysk@yfukai.net

† kat@kaztake.org

- [1] T. Sasamoto, J. Phys. A: Math. Gen. **38**, L549 (2005).
- [2] A. Borodin, P. L. Ferrari, M. Prähofer, and T. Sasamoto, J. Stat. Phys. **129**, 1055 (2007).
- [3] M. Prähofer and H. Spohn, J. Stat. Phys. **108**, 1071 (2002).
- [4] J. Baik, P. L. Ferrari, and S. Péché, Commun. Pure Appl. Math. **63**, 1017 (2010).
- [5] J. Quastel and D. Remenik, in *Topics in Percolative and Disordered Systems* (Springer, New York, NY, 2014) pp. 121–171.
- [6] K. A. Takeuchi and M. Sano, J. Stat. Phys. **147**, 853 (2012).
- [7] P. L. Ferrari and H. Spohn, Symmetry Integrability Geom. Methods Appl. **12**, 074 (2016).
- [8] J. De Nardis, P. Le Doussal, and K. A. Takeuchi, Phys. Rev. Lett. **118**, 125701 (2017).
- [9] K. Johansson, Probab. Theory Related Fields **175**, 849 (2019).
- [10] K. Johansson and M. Rahman, Commun. Pure Appl. Math. (2021), 10.1002/cpa.21980.
- [11] Z. Liu, (2019), arXiv:1907.09876.
- [12] M. Prähofer and H. Spohn, J. Stat. Phys. **115**, 255 (2004).
- [13] F. Bornemann, Math. Comput. **79**, 871 (2010).